Direct suppression of host gluconeogenesis by Trypanosoma brucei

Luísa Figueiredo

luisa.figueiredo@gimm.pt

Gulbenkian Institute for Molecular Medicine

Abdulbasit Amin

Gulbenkian Institute for Molecular Medicine

João Colaço

Gulbenkian Institute for Molecular Medicine

Henrique Machado

ICVS-Life and Health Sciences Research Institute, School of Medicine, University of Minho

Helena Nunes-Cabaço

Gulbenkian Institute for Molecular Medicine https://orcid.org/0000-0001-7213-2879

Sandra Trindade

Gulbenkian Institute for Molecular Medicine

Philipp Scherer

The University of Texas Southwestern Medical Center https://orcid.org/0000-0003-0680-3392

Sara Silva Pereira

Universidade Catolica Portuguesa https://orcid.org/0000-0002-6590-6626

Article

Keywords:

Posted Date: January 13th, 2026

DOI: https://doi.org/10.21203/rs.3.rs-8369960/v1

Additional Declarations: There is **NO** Competing Interest.

Direct suppression of host gluconeogenesis by *Trypanosoma brucei*

Abdulbasit Amin[1,2], João Colaço[1], Henrique Machado[3,4], Helena Nunes-Cabaço[1], Sandra Trindade[1], Philipp E Scherer[5,6], Sara Silva Pereira[7], Luisa M Figueiredo[1]*

[1] Gulbenkian Institute for Molecular Medicine, Edificio Egas Moniz, Avenida Professor Egas Moniz, 1649-028 Lisbon, Portugal.
[2] Department of Physiology, Faculty of Basic Medical Sciences, University of Ilorin, Ilorin, Nigeria.
[3] ICVS-Life and Health Sciences Research Institute, School of Medicine, University of Minho, 4710-057 Braga, Portugal.
[4] ICVS/3Bs-PT Government Associate Laboratory, 4710-057 Braga, Portugal
[5] Touchstone Diabetes Center, University of Texas Southwestern; Medical Center, Dallas, TX, USA
[6] Department of Internal Medicine and Department of Cell Biology, University of Texas Southwestern Medical Center, Dallas, TX, USA
[7] Católica Biomedical Research Centre, Católica Medical School, Universidade Católica Portuguesa, Oeiras, Portugal

*Corresponding author: luisa.figueiredo@gimm.pt

ABSTRACT

The cause of hypoglycaemia in African trypanosomiasis remains unresolved. We found that infected mice show normal carbohydrate digestion, intestinal glucose absorption, and tissue glucose uptake, but a profound reduction of host glucose production via gluconeogenesis. Liver transcriptomics uncovered coordinated repression of gluconeogenic pathways alongside inflammatory activation. Infection of $Rag2^{-/-}$ mice showed that adaptive immunity contributes only minimally to suppression of host gluconeogenesis. In contrast, therapeutic parasite clearance completely restored host glycaemia and gluconeogenesis despite persistent immune activation. These results demonstrate that live parasites directly repress gluconeogenesis *in vivo*. Using a co-culture assay, we showed that *T. brucei* is sufficient to directly repress gluconeogenic gene expression in primary hepatocytes *in vitro*. Finally, we found that providing glycerol in drinking water to infected animals stimulated gluconeogenesis, elevated glycaemia, and improved survival without impacting parasitaemia. This study reveals a previously unrecognised pathogenic strategy in which a eukaryotic parasite directly suppresses host gluconeogenesis.

INTRODUCTION

Infectious diseases impose significant metabolic challenges on hosts, requiring adaptive changes to maintain energy balance while simultaneously combating pathogens (1–4). These adaptations often involve mobilising dietary and endogenous energy reserves, such as glycogen in the liver (5,6) and triglycerides in white adipose tissue (7,8), to ensure a continuous supply of essential energy substrates like glucose and lipids for an appropriate immune response (9–12). However, pathogens exploit these resources for their own survival, creating a metabolic tug-of-war that shapes disease outcomes. For example, bloodstream

forms of Trypanosoma brucei predominantly rely on glucose as a carbon source (13,14) and retain the ability to metabolise alternative substrates such as glycerol (15,16). Similarly, Plasmodium spp. depend on host haemoglobin for amino acids (17), while Leishmania spp. utilize lipid-derived nutrients from host macrophages (18). These interactions reflect competing metabolic priorities between host and pathogen, where resource allocation decisions critically determine infection outcomes.

Glucose is a fundamental energy substrate for essential metabolic activities, serving as the primary fuel for ATP production via glycolysis and oxidative phosphorylation. Yet, it also provides a carbon skeleton for biosynthesis and redox balance in critical host tissues/organs, such as the immune, brain or muscle cells. Normal blood glucose level is maintained through a balance between exogenous carbohydrate ingestion and digestion in the gut, glucose absorption via the small intestine, storage of excess circulating glucose (in organs such as the liver, muscle, and adipose tissues), and endogenous production of glucose from organs like the liver and the kidney to prevent hypoglycaemia during fasting or starvation (19–22).

Glucose is produced endogenously from the hydrolysis of glycogen stores in the liver via glycogenolysis (22). In prolonged fasting or starvation, and after glycogen depletion, gluconeogenesis is activated to maintain blood glucose levels (22). Gluconeogenesis utilises non-carbohydrate precursors, including lactate, pyruvate, glycerol, and amino acids, to produce glucose. This pathway is energetically costly and occurs primarily in the liver and the kidneys (23). Gluconeogenic precursors are converted to glucose via pathway-specific enzymes: phosphoenolpyruvate carboxykinase (*Pck1*), fructo-1,6-bisphosphatase-1 (*Fbp1*), and glucose-6-phosphatase (*G6pc*). Gluconeogenesis is hormonally regulated: insulin suppresses it, while glucagon and glucocorticoids activate it (24,25).

In many infectious diseases, gluconeogenesis itself becomes a target of host metabolic reprogramming. In sepsis and malaria, labile heme released from the host's red blood cell lysis inhibits gluconeogenesis in the liver, contributing to hypoglycaemia (26,27). In Tuberculosis, type I immune response represses both the expression of key gluconeogenic genes and hepatic gluconeogenesis (28). Together, these findings demonstrate that the suppression of gluconeogenesis is a recurring feature of host responses to infection, although the underlying mechanisms vary across pathogens.

In infections by *Trypanosomes*, decreased blood glucose level (hypoglycaemia) is a commonly reported symptom (5,29–31). While hypoglycaemia can be life-threatening, its aetiology, the mechanism(s) of its induction, and relevance to host survival in African Trypanosomiasis, are poorly understood. Here, we sought to disentangle the contribution of *T. brucei*'s glucose consumption and host immunometabolic reprogramming to hypoglycaemia in African trypanosomiasis. We show that the adaptive immune-mediated response is necessary but not sufficient to impair *T. brucei*-associated suppression of gluconeogenesis. Consistently, the presence of parasites is necessary *in vivo* and sufficient *in vitro* to directly suppress hepatocyte gluconeogenesis. Providing glycerol, a gluconeogenic precursor, to *T. brucei*–infected mice enhances glycaemia and prolongs survival without altering parasitemia, demonstrating that infection-induced hypoglycaemia arises primarily from host metabolic suppression

rather than parasite glucose consumption. Enhancing endogenous glucose production improves host fitness independently of pathogen control, revealing a novel mechanism of disease tolerance in African trypanosomiasis.

RESULTS

Endogenous glucose production is impaired in infected mice

Hypoglycaemia has been observed in humans and mice infected with *T. brucei* (31,32). We therefore seek to better understand the dynamics of glycaemia in mice infected with *T. brucei*. We assessed glycaemia in the fed state (when mice had access to food *ad* libitum) as infection progressed (Figure 1A). We found that in infected mice, glycaemia progressively declined with infection, reaching its lowest level on day 7 post-infection (Figure 1A). Food intake of infected mice also decreased gradually (Figure 1B), potentially contributing to the observed hypoglycaemia early in infection (Figure 1A). However, glycaemia remained significantly lower after day 7 post-infection (Figure 1A), despite restored food intake (Figure 1B) ($p<0.001$).

To mitigate the effect of discrepant food intake on glycaemia, we measured glycaemia in fasting conditions. For that, mice were fasted for either 6 hours or overnight before assessing glycaemia (Figure 1C). After acute fasting (6 h), infected mice showed significantly lower glycaemia than uninfected mice on days 7 ($p<0.0001$), 14 ($p<0.0001$), and 21 ($p<0.0001$) post-infection. After an overnight fast, infected mice also showed significantly lower glycaemia than uninfected mice on days 7 ($p<0.0001$), 14 ($p<0.001$), and 21 ($p<0.05$) post-infection. These observations show that infection disrupts baseline glucose homeostasis independently of anorexia, with the defect becoming more evident during prolonged fasting.

In the mammalian host, dysregulation of glycaemia could result from disruption in at least one of these layers of glucose regulation: 1. digestion and absorption in the intestine, 2. glucose uptake by organs, or 3. endogenous glucose production by gluconeogenesis. To test if digestion and absorption were affected, we performed a sucrose tolerance test (Figure 1D, Supplementary Figure 1B). We administered sucrose orally to fasted mice (uninfected and infected) and monitored the rate of change in blood glucose for 120 min, measured as a percentage of baseline fasting glucose (Figure 1D, Supplementary Figure 1B). We tested mice infected for 7, 14, or 21 days post-infection, a proxy for early, mid, and late stages of the disease, respectively. Non-infected mice show a sharp increase in glycaemia that peaks in the first 15 minutes, which gradually reduces due to insulin secretion and uptake by tissues (33). Infection had no impact on blood glucose dynamics in response to a bolus of sucrose (Figure 1D, Supplementary Figure 1B), indicating that glucose digestion and absorption in the intestine are not impaired during *T. brucei* infection.

Next, we assessed whether the glucose uptake by organs was compromised in infected mice at the same disease stages. Glucose was administered intraperitoneally to infected and uninfected fasted mice, and the rate of change in blood glucose was monitored, as described above. Infected mice exhibited a higher peak glycemic response (30min) relative to baseline glucose (statistically significant, $p<0.05$ on days 7 post-infection), suggesting a faster rate of glucose

absorption into the bloodstream in infected mice on day 7 (Figure 1E, Supplementary Figure 1C). However, glucose clearance rates (measured from 30-120 min) were comparable to uninfected controls (Figure 1E, Supplementary Figure 1C). These results indicate that glucose clearance is not compromised at any stage of infection.

Finally, to assess the capacity of infected mice to produce glucose from gluconeogenic precursors (such as pyruvate and glycerol), we administered pyruvate or glycerol intraperitoneally to infected and uninfected fasted mice and assessed the rate of change in blood glucose as described above. Infection with *T. brucei* had no impact on the rate of change in glycaemia on day 7 post-infection in response to pyruvate or glycerol administration (Figure 1F & G). However, a significant decrease in the rate of glucose production on days 14 ($p<0.01$) and 21 ($p<0.0001$) post-infection was observed in response to pyruvate. A similar result was observed when we administered glycerol on days 14 ($p<0.01$) and 21 ($p<0.001$) post-infection (Figure 1G, Supplementary Figure 1E). The results suggest that infected animals are unable to produce normal levels of glucose via gluconeogenesis from these substrates.

Collectively, these results demonstrate that *T. brucei*–infected mice maintain normal intestinal carbohydrate digestion, absorption, and glucose clearance, but exhibit a marked defect in endogenous glucose production via gluconeogenesis.

Figure 1: Endogenous glucose production is impaired in mice infected with *T. brucei*

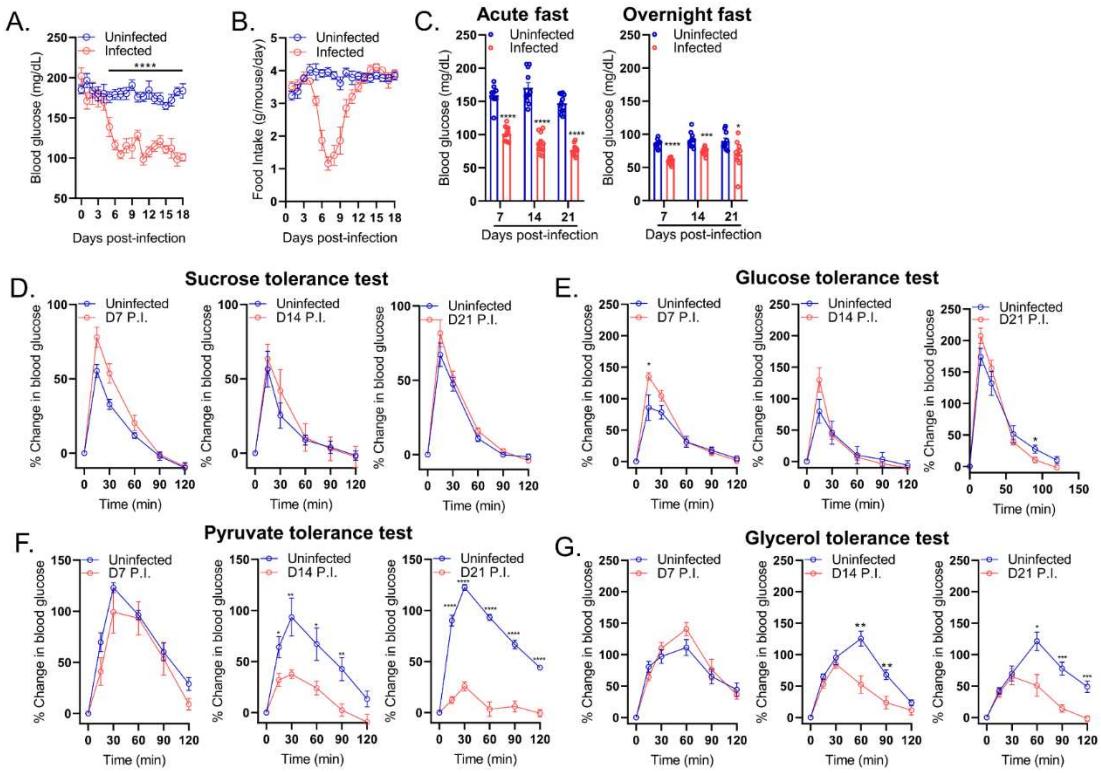

Figure 1: **Endogenous glucose production is impaired in mice infected with *Trypanosoma brucei*. A.** Dynamics of blood glucose in the fed state in uninfected and mice infected with *T. brucei*. n = 10 uninfected and n = 8 infected mice were

examined over 2 independent experiment. **B.** Food intake of uninfected and mice infected with *T. brucei*. **C.** Acute (6h) and overnight fasting blood glucose levels of uninfected mice and mice infected with *T. brucei* for 7, 14, & 21 days. n = 11 each for uninfected and infected mice on day 7 and 14 post-infection, and n = 9 for infected mice on day 21 post-infection, examined over 2 independent experiments. **D.** Percentage change from basal blood glucose during the sucrose tolerance test for uninfected mice and mice infected with *T. brucei* for 7, 14, & 21 days. n = 6 uninfected and n = 6 infected mice on day 7, n = 7 uninfected and n = 9 infected mice on day 14, and n = 6 uninfected and n = 6 infected mice on day 21 post-infection, examined over 2 independent experiment. **E.** Percentage change from basal blood glucose during glucose tolerance test for uninfected mice and mice infected with *T. brucei* for 7, 14, & 21 days. n = 6 uninfected and n = 6 infected mice on day 7, n = 6 uninfected and n = 8 infected mice on day 14, and n = 8 uninfected and n = 8 infected mice on day 21 post-infection, examined over 2 independent experiments. **F.** Percentage change from basal blood glucose during the pyruvate tolerance test for uninfected mice and mice infected with *T. brucei* for 7, 14, & 21 days. n = 6 uninfected and n = 6 infected mice on day 7, n = 6 uninfected and n = 8 infected mice on day 14, and n = 6 uninfected and n = 6 infected mice on day 21 post-infection, examined over 2 independent experiments. **G.** Percentage change from basal blood glucose during glycerol tolerance test for uninfected mice and mice infected with *T. brucei* for 7, 14, & 21 days. n = 8 uninfected and n = 8 infected mice on day 7, n = 6 uninfected and n = 6 infected mice on day 14, and n = 6 uninfected and n = 5 infected mice on day 21 post-infection were examined over 2 independent experiment. Error bars represent the S.E.M. $*P < 0.05$, $**P < 0.01$, $****P < 0.0001$. Statistical source data contain additional parameters.

Endogenous glucose production is impaired despite adequate availability of gluconeogenic substrates

Gluconeogenesis requires non-carbohydrate precursors such as lactate, pyruvate, and glycerol (20). Given the decrease in endogenous glucose production in infected mice, we hypothesised that reduced gluconeogenesis could be due to lower levels of these precursors during a *T. brucei* infection. To test this, we quantified the levels of lactate, pyruvate and glycerol. The blood levels of lactate were significantly elevated on days 14, 21, and 28 ($p<0.01$, $p<0.05$, $p<0.05$, respectively) post-infection relative to blood lactate levels in uninfected mice (Figure 2A). This effect has been reported previously and attributed to the parasites' high glycolytic rate (29). On the other hand, however, no significant changes were observed in the levels of pyruvate or glycerol (Figure 2B-C). These observations show that the decrease in endogenous glucose production in the infected mice is not a result of low levels of gluconeogenic precursors.

In addition to substrate availability, gluconeogenesis is also regulated by hormones: glucagon stimulates gluconeogenesis, while insulin inhibits it (24,34). We hypothesised that reduced gluconeogenesis could be due to lower levels of glucagon or higher levels of insulin during infection. Quantification of serum levels of insulin and glucagon showed that glucagon availability increased progressively with infection and rose to significant levels on days 21 ($p<0.01$) and 28 ($p<0.01$) post-infection (Figure 2D), while no change was observed in the levels of insulin

(Figure 2E). These results show that reduced gluconeogenesis in infected animals is not due to a decrease in the levels of glucagon nor an increase in the levels of insulin. In fact, the increase in glucagon, which in normal conditions would promote gluconeogenesis, might represent a failed attempt by the host to boost endogenous glucose production.

These results indicate that the impairment in gluconeogenesis in *T. brucei*-infected mice is not due to substrate limitation, nor disruption in the secretion of major hormones involved in the regulation of gluconeogenesis.

Figure 2: Endogenous glucose production is impaired despite adequate availability of gluconeogenic substrates

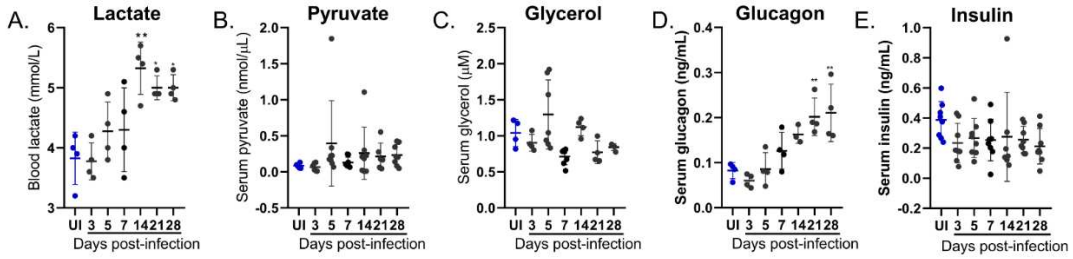

Figure 2: **Endogenous glucose production is impaired despite adequate availability of gluconeogenic substrates. A.** Blood lactate levels in uninfected and *T. brucei*-infected mice. n = 4 uninfected and n = 4 infected mice. **B.** Serum pyruvate levels in uninfected and *T. brucei*-infected mice. n = 8 for uninfected and infected mice on days 5, 7, 14 and 28, and n = 6 for infected mice on days 3 and 21 examined over 2 independent experiments. **C.** Serum glycerol levels in uninfected and *T. brucei*-infected mice. n = 4 for uninfected and infected mice on days 3, 14, 21 and 28, and n = 7 for infected mice on days 5 and 7, examined over 2 independent experiments. **D.** Serum glucagon levels in uninfected and *T. brucei*-infected mice. n = 4 for uninfected and infected mice on days 3, 5, 7, 14, and 21, and n = 3 for infected mice on days 28. **E.** Serum insulin levels in uninfected and *T. brucei*-infected mice. n = 8 for uninfected and infected mice on examined over 2 independent experiments. Error bars represent the S.E.M. **P* < 0.05, ***P* < 0.01, *****P* < 0.0001. Statistical source data contain additional parameters.

Liver transcriptome reveals upregulation of inflammatory genes and downregulation of metabolic genes

As the liver controls systemic glucose homeostasis, including gluconeogenesis, we hypothesised that this organ may be affected during infection. We performed mRNA sequencing throughout infection (days 0, 6, 10, and 22 post-infection) to identify infection-induced perturbations in gene expression programs.

Multidimensional scaling (MDS) of hepatic transcriptomes demonstrated a clear response to infection, starting from day 6 post-infection (dimension 1, 50% variance) (Figure 3A). There was also a clear temporal distinction throughout infection, as transcriptomes from days 10 and 22 post-infection, not only clustered together and away from days 6, but also repositioned closer to uninfected controls along dimension 2. This suggests a stable infection-associated transcriptional state by day 10 that persisted through chronic infection (Figure 3A).

Differential gene expression analysis of the liver transcriptomes at day 6 post-infection and uninfected revealed 742 significantly upregulated and 152 downregulated genes ($\log_2$ FC ≥1, adj. p-value < 0.05) (Supplementary File 1). By day 10 post-infection, 633 genes were significantly upregulated, and 167 genes were downregulated relative to the uninfected mice. At the later stage of infection, day 22, 730 genes were significantly upregulated, and 117 genes were downregulated (Figure 3B).

To better dissect the temporal evolution of the hepatic transcriptional response to infection, we visualised the relative deviation of gene expression across these time points (day 6, 10, and 22 postinfection) using a radial deviation plot (Figure 3C). This revealed a temporal progression in hepatic gene expression during *T. brucei* infection, with distinct spatial patterns reflecting both the magnitude and timing of transcriptional changes. While the majority of differentially expressed genes are common between days 6, 10, and 22 post-infection (with similar effect sizes and statistical significance), and are therefore centrally located in the graph, there are differences in the expression profiles of the liver at specific stage of disease. These include genes that are exclusively differentially regulated at day 6 post-infection, such as albumin (*Alb*) and solute carrier family 2 (facilitated glucose transporter) member 2 (*Slc2a2*), indicating early transient suppression of hepatocyte metabolic functions. Genes exclusively regulated at day 10 post-infection include glutathione S-transferase alpha 2 and 4 (*Gsta2/4*) and HECT domain E3 ubiquitin protein ligase 2 (*Hectd2os),* suggesting progressive repression of oxidative stress responses. Genes more strongly regulated at day 22 post-infection include the upregulated immune effectors CXCL13 and tumour necrosis factor receptor superfamily member 17 (Tnfrsf17). Lysozyme M, also involved in chronic inflammation, is upregulated at all time points post-infection; however, the largest effect size ($\log_2$ FC = 2.85) is observed at day 22. Notably, metabolic genes, such as cysteine sulfinic acid decarboxylase (*Csad*), become once again strongly downregulated, despite a partial recovery in expression at day 10 post-infection, revealing host failure to recover hepatic homeostasis.

Overall, GO term enrichment analysis of the differentially expressed genes of infected liver at all stages of disease revealed a general upregulation in genes associated with immune and inflammatory processes, including the toll-like receptor signalling pathway**,** innate immune response**,** cytokine-mediated signalling**,** B cell receptor signalling, and leukocyte chemotaxis (Figure 3D). These findings indicate robust activation of both innate and adaptive immune pathways in the infected liver. On the other hand, downregulated genes were overwhelmingly associated with metabolic functions and a broad spectrum of oxidoreductase and monooxygenase activities, including heme binding (Figure 3D).

To test if genes encoding for the gluconeogenesis pathway are transcriptionally downregulated, we performed gene set enrichment analysis (GSEA), which evaluates whether predefined groups of functionally related genes show coordinated shifts in expression across experimental conditions. Applied to the gluconeogenesis gene set, GSEA revealed a clear negative enrichment in infected livers (Figure 3E), indicating that gluconeogenesis as a pathway is broadly and consistently suppressed during *T. brucei* infection.

Together, these data reveal that *T. brucei* infection causes significant transcriptional reprogramming of the liver, characterised by a strong and continuous immune activation and suppression of key metabolic processes, including the gluconeogenesis pathway.

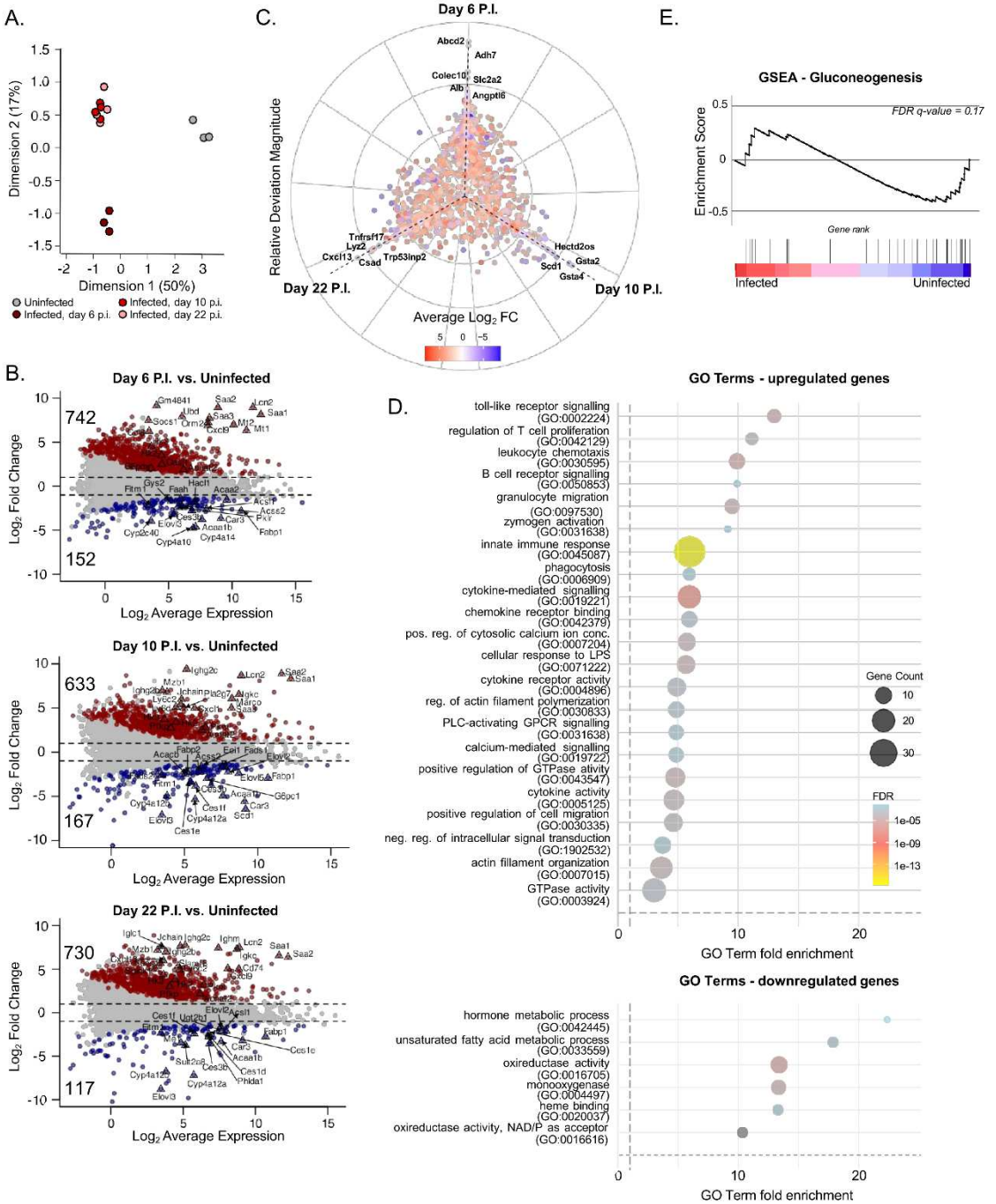

Figure 3: Liver transcriptome reveals upregulation of inflammatory gene and downregulation of metabolic genes

Figure 3: **Liver transcriptome of mice infected with** *T. brucei* **reveals upregulation of inflammatory genes and downregulation of metabolic genes. A.** MDS plot of liver transcriptomes comparing uninfected mice and *T. brucei*-infected mice at days 6, 10, and 22 post-infection. Axes represent the leading log fold change of dimensions 1 or 2, with explained variance indicated in brackets. n = 3 each of uninfected and day 6 infected mice, and n = 4 each of day 10 and 22 infected mice.

B. MA plot showing differential expression in the liver of mice infected with *T. brucei* for 6 (A), 10 (B), or 22 (C) days post-infection compared to uninfected controls, expressed as Log_2 fold change and Log_2 average transcript counts per million transcripts. Red and blue indicate up- and downregulation compared to uninfected mice, respectively. **C.** Polar plot of differential gene expression across days 6, 10, 22 post-infection relative to uninfected. Each point represents a gene significantly differentially expressed in at least one time point (adjusted $p < 0.05$). The plot is in polar coordinates, with three fixed axes corresponding to day 6 (0°), day 10 (120°), and day 22 (240°). The angle of each point indicates the timepoint(s) driving the deviation in expression: points align toward the axis of the timepoint with the strongest deviation, or between axes if multiple timepoints contribute. The radius represents the overall magnitude of deviation between timepoints, calculated as the Euclidean distance of the weighted relative deviations (weighted by $-\log_{10}$ adjusted *p*-value) and displayed on a logarithmic scale. Colour indicates the average $\log_2$ fold change across timepoints (red = upregulated, blue = downregulated). Dashed grey lines mark the timepoint axes, and the top 15 genes by radius are labelled. **D.** Bubble chart displaying significantly enriched Gene Ontology (GO) terms (FDR < 0.05) in *T. brucei*-infected versus uninfected liver samples (all timepoints combined). Bubble size represents the number of differentially expressed genes contributing to each GO term. Bubble order represents fold enrichment as shown in the horizontal axis. Bubbles are colour-coded according to the FDR value. **E.** Gene Set Enrichment Analysis (GSEA) of gluconeogenesis-associated genes in the liver of infected mice on day 6 post-infection.

Gluconeogenesis is downregulated in the liver, kidney, and isolated hepatocytes of infected mice

Our comprehensive, whole-liver transcriptomic analysis revealed widespread downregulation of metabolic genes, including those involved in gluconeogenesis. While multiple cell types might contribute to this phenotype, the expression of gluconeogenic genes is largely attributed to the hepatocytes. Given that bulk liver RNA reflects a mixture of parenchymal and non-parenchymal cells, we hypothesise that the observed transcriptional repression of gluconeogenesis might originate specifically from hepatocytes; next, we directly measured gluconeogenic gene expression in whole liver and in purified hepatocytes to determine whether this defect is hepatocyte-intrinsic.

To test this, we collected and performed RT-qPCR on livers of uninfected mice and mice infected for 3, 5, 7, 14, 21, and 28 days to evaluate the levels of the gluconeogenic genes, *G6pc* (glucose-6-phosphatase), and *Pck1* (phosphoenolpyruvate carboxykinase) (Figure 4 B-C). We observed no significant change in the expression of *G6pc* or *Pck1* during the early phase of infection (up to day 5 and day 7 post-infection, respectively), but both genes showed a marked decrease from day 7 onward (*G6pc*) and day 14 onward (*Pck1*) (Figure 4B–C). Linear regression analysis revealed a strong negative association between time post-infection and the expression of both genes (*G6pc*, slope = −0.0438, $R^2 = 0.6977$, p = 0.0002; *Pck1*, slope = −0.0475, $R^2 = 0.6510$, p = 0.0005), indicating a progressive

decline in hepatic gluconeogenic capacity over the course of infection (Figure 4B–C).

To determine whether these whole-liver expression changes reflected hepatocyte-specific effects rather than contributions from non-parenchymal cells (such as resident and infiltrated immune cells), we isolated hepatocytes from uninfected and infected mice at day 14 post-infection and performed targeted RT-qPCR analysis. We confirmed that the suppression of gluconeogenic enzymes was indeed hepatocyte-autonomous, with infected hepatocytes showing significant reductions in *G6pc* ($P<0.05$) and *Pck1* ($p<0.05$) compared to hepatocytes from uninfected mice (Figure 4D). This hepatocyte-specific repression supports an intrinsic reprogramming of the liver's metabolism.

The kidney has been shown to compensate for the impaired capacity of the liver to produce glucose in some disease contexts (35). To assess whether this is the case in *T. brucei* infection, we quantified the transcript levels of the gluconeogenic genes *G6pc* and *Pck1* in the kidney. Like the liver, renal *G6pc* levels decrease as infection progresses. A linear regression analysis revealed a significant negative relationship between time post-infection and renal *G6pc* (slope = −0.0195, $R^2 = 0.410$, $p = 0.0137$), indicating a modest but consistent reduction in *G6pc* levels as infection progressed (Figure 4E). Renal *Pck1* expression remained unchanged in mice infected for up to 7 days. However, its expression decreased on the subsequent days. In addition, there is a significant negative correlation between renal *Pck1* expression and time post-infection (slope = –0.0240, $R^2 = 0.6541$, $p = 0.0005$), indicating a progressive decline in expression over time (Figure 4F).

Taken together, these results demonstrate that *T. brucei* infection causes profound and progressive suppression of hepatic gluconeogenesis through coordinated transcriptional repression of the major gluconeogenic genes, without compensatory activation of renal gluconeogenic pathways.

Figure 4: Gluconeogenesis is downregulated in liver, kidney and isolated hepatocytes of infected mice.

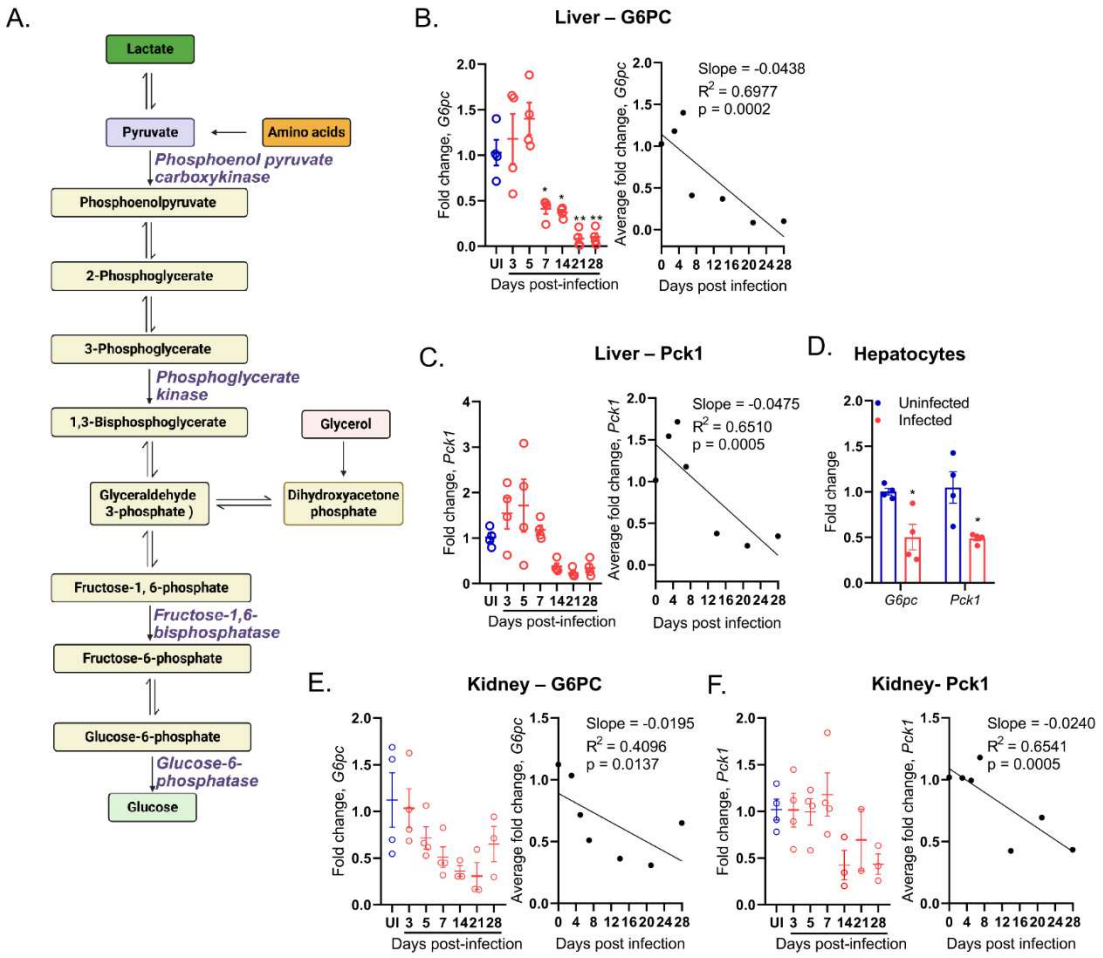

Figure 4: **Gluconeogenesis is impaired in infected hepatocytes**. **A.** Schematic**,** gluconeogenesis pathway showing various steps involved in the conversion of lactate, pyruvate, amino acids, and glycerol to glucose and the enzymes involved in catalysing the irreversible steps. **B.** RT-qPCR quantification and the linear regression analysis of the gluconeogenic gene, *G6pc,* in the liver from uninfected (UI) mice and mice infected with *T. brucei* for 3, 5, 7, 14, 21, and 28 days. n = 4 each of uninfected and infected mice. **D.** RT-qPCR quantification and the linear regression analysis of the gluconeogenic gene, *Pck1,* in the liver from uninfected (UI) mice and mice infected with *T. brucei* for 3, 5, 7, 14, 21, and 28 days. n = 4 each of uninfected and infected mice. **D.** RT-qPCR quantification of gluconeogenic genes, *G6pc* and *Pck1*in hepatocytes collected from the liver of uninfected mice and mice infected (for 14 days) with *T. brucei*. n = 4 each of uninfected and infected mice. **E.** RT-qPCR quantification and the linear regression analysis of the gluconeogenic gene, *G6pc,* in the kidney from uninfected (UI) mice and mice infected with *T. brucei* for 3, 5, 7, 14, 21, and 28 days. n = 4 each of uninfected and infected mice except infected days 14, 21, & 28 (n = 3). **F.** RT-qPCR quantification and the linear regression analysis of the gluconeogenic gene, *Pck1,* in the kidney from uninfected (UI) mice and mice infected with *T. brucei* for 3, 5, 7, 14, 21, and 28 days. n = 4 each of uninfected and infected mice except infected day 14, 21, & 28 (n

= 3). Error bars represent the S.E.M. *$P < 0.05$, **$P < 0.01$, ****$P < 0.0001$. Statistical source data contain additional parameters.

Adaptive immunity selectively constrains gluconeogenesis

Our results showed that endogenous glucose production in infected mice is functionally impaired in the mid and late stages of infection with *T. brucei*. The proinflammatory immune response characteristic of these stages is driven largely by the adaptive immune compartment and could drive the observed impairment in hepatic glucose production, as observed in tuberculosis (28).

To understand the contribution of the adaptive immune response, we used Rag2 knock-out mice ($Rag2^{-/-}$), which lack mature B and T lymphocytes. We followed infection for 14 days and found no difference in blood glucose levels between $Rag2^{-/-}$ and WT mice in the fed state (Figure 5A) despite sustained hyperparasitamia in the $Rag2^{-/-}$ mice (Figure 5B). Although blood glucose levels in $Rag2^{-/-}$ mice tended to be slightly higher after acute fasting (6 h), this difference was not statistically significant, and glucose levels were similar to those of infected wild-type mice after prolonged (overnight) fasting (Figure 5C). Next, we performed glycerol and pyruvate tolerance tests to assess gluconeogenesis in these mice (Figure 5 D&E). As shown in Figure 5D, infected $Rag2^{-/-}$ mice have a significantly ($p<0.01$) higher glycaemic response to glycerol administration relative to the infected WT mice (Figure 5D). However, no differences were observed between infected WT and infected $Rag2^{-/-}$ in the glycaemic response to pyruvate (Figure 5E). The contrasting response to glycerol and pyruvate may indicate that the adaptive immunity selectively constrains the glycerol→glucose arm of gluconeogenesis, while the mitochondrial/pyruvate-dependent branch is comparably suppressed in both genotypes.

In summary, these findings suggest that while the adaptive immune response contributes to the repression of gluconeogenesis, it is not sufficient on its own to account for the full metabolic impairment observed during infection, indicating that other mechanisms likely play a dominant role.

Figure 5: Adaptive immune response selectively constrains gluconeogenesis

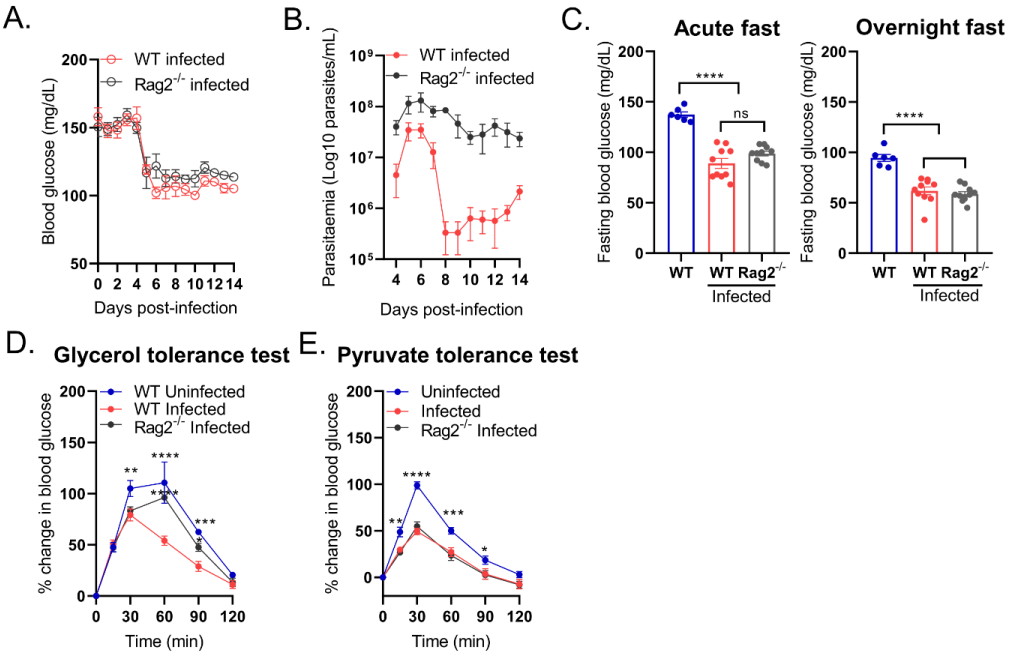

Figure 5: **Adaptive immune response selectively constrains gluconeogenesis**. **A.** Dynamics of blood glucose levels in the fed state for WT and Rag2$^{-/-}$ mice infected with *T. brucei*. n = 7 WT and n = 8 Rag2$^{-/-}$ mice examined over 2 independent experiments. **B.** Parasitaemia in WT and Rag2KO mice infected with *T. brucei*. n = 6 each of WT and Rag2$^{-/-}$ infected mice. **C.** Acute (6h) and overnight fasting blood glucose levels of WT uninfected, and WT and Rag2KO mice infected with *T. brucei*. n = 6 infected mice, and n = 10 each of WT and Rag2$^{-/-}$ infected mice examined over 2 independent experiment. **D.** Change in blood glucose during glycerol tolerance test in WT uninfected, and WT and Rag2KO mice infected with *T. brucei*. n = 6 WT uninfected, and n = 8 each of WT and Rag2$^{-/-}$ infected mice, examined over 2 independent experiment. **G.** Change in blood glucose during the pyruvate tolerance test in WT uninfected, and WT and Rag2$^{-/-}$ mice infected with *T. brucei*. n = 6 WT uninfected, and n = 8 each of WT and Rag2$^{-/-}$ infected mice examined over 2 independent experiments. Error bars represent the S.E.M. *$P < 0.05$, **$P < 0.01$, ****$P < 0.0001$. Statistical source data contain additional parameters.

T. brucei is sufficient to inhibit gluconeogenesis

Given the modest and only partial contribution of adaptive immunity to the repression of gluconeogenesis, we hypothesised that *T. brucei* directly inhibits hepatic glucose production. To test this, infected mice were treated intravenously with the anti-trypanosomal drug, melarsoprol or its vehicle at day 14 post-infection (Figure 6A). We predict that a few days after melarsoprol treatment, parasite load should sharply decrease while immune response should remain active within a few days after treatment. This setting would allow us to delineate the role of the parasites in regulating gluconeogenesis from the proinflammatory immune response associated with the infection.

Parasitemia was undetectable after treatment, confirming effective parasite clearance in the blood (Figure 6B). To determine whether adaptive immune activation persisted after parasite elimination, we quantified circulating $CD4^+$ and $CD8^+$ T cells, as well as effector/effector memory T cell (T_{EM}) subsets, on day 14 (pre-treatment) and day 18 (four days post-treatment). The ratio of cell frequencies between these two time points showed no significant change (Figure 6C; Supplementary Figure 3B-C), indicating that adaptive immunity remained active despite parasite clearance.

We next assessed the impact of parasite elimination on systemic glucose regulation. Following melarsoprol administration, fed-state glycaemia progressively increased, reaching significantly higher levels than in untreated infected mice on days 15–18 post-infection (Figure 6D). By day 18, both acute (6 h) and overnight fasting blood glucose levels in melarsoprol-treated mice had returned to similar levels as those observed in uninfected controls (Figure 6E). Melarsoprol-treated infected animals displayed a similar glycemic response to glycerol and pyruvate as observed in uninfected mice, a significantly higher glycemic response compared to untreated infected mice (Figure 6F).

These findings indicate that the presence of live parasites is necessary for the maintenance of hypoglycaemia and suppression of hepatic glucose production *in vivo*. Together with the $Rag2^{-/-}$ data, we show that while the adaptive immune response contributes modestly to metabolic repression, the presence of parasites exerts a more dominant, parasite-intrinsic control over hepatic gluconeogenesis, establishing the parasite as the central determinant of infection-induced hypoglycaemia.

Figure 6: *T. brucei* is suficient to inhibit gluconeogenesis

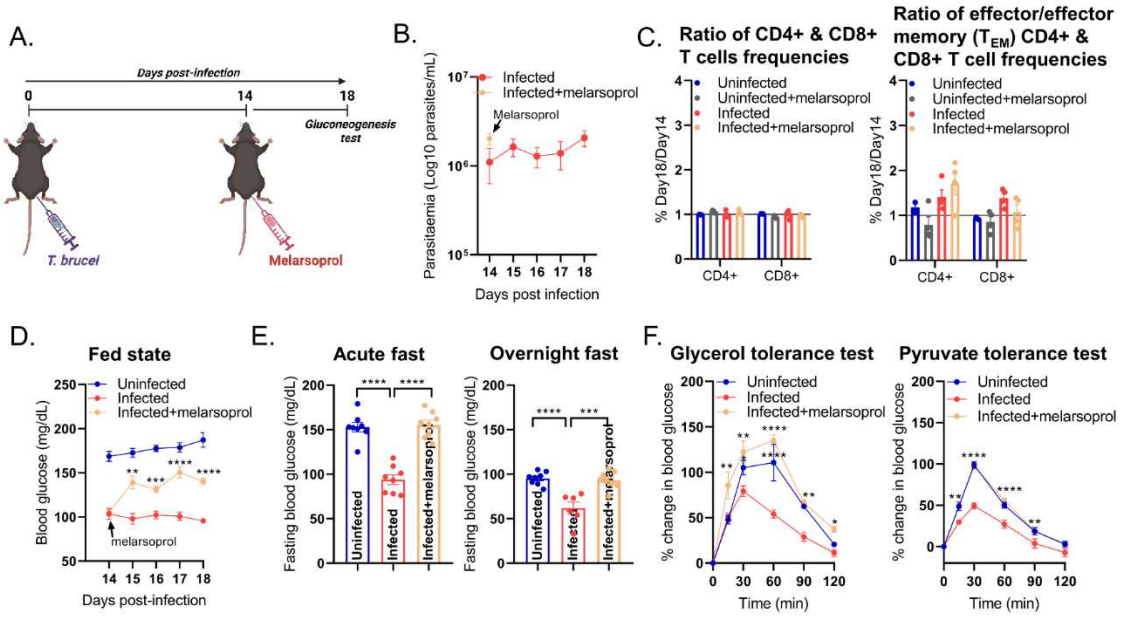

Figure 6: ***T. brucei* is sufficient to inhibit gluconeogenesis**. **A.** Schematic showing how Parasitaemia in infected WT mice was cleared using the antitrypanosome drug, melarsoprol. **B.** Parasitaemia in infected mice treated with or without melarsoprol. n = 6 infected and n = 8 infected and treated with melarsoprol. **C.** Ratio of CD4+ & CD8+ T cell and of effector/effector memory (T_{EM}) CD4+ & CD8+ T cell frequencies

in uninfected and infected mice, treated with or without melarsoprol on day 18 vs day 14 post-infection. n = 3 uninfected mice, and n = 4 mice each for uninfected mice treated with melarsoprol, infected mice, and infected mice treated with melarsoprol. **D.** Dynamics of blood glucose in the fed state for uninfected and infected WT mice treated with or without melarsoprol. n = 8 uninfected mice, n = 6 infected mice, and n = 8 infected mice treated with melarsoprol. **E.** Acute (6h) and overnight fasting blood glucose levels of uninfected and infected mice treated with or without melarsoprol. n = 8 mice each of uninfected, infected, and infected mice treated with melarsoprol. **F.** Glycerol tolerance and pyruvate tolerance tests in infected mice treated with or without melarsoprol. n = 8 infected and n = 8 infected and treated with melarsoprol. Error bars represent the S.E.M. **P* < 0.05, ***P* < 0.01, *****P* < 0.0001. Statistical source data contain additional parameters.

T. brucei directly suppresses glucose production in hepatocytes

To determine whether *T. brucei* directly modulates glucose production in hepatocytes, we co-cultured primary hepatocytes isolated from uninfected wild-type mice with live parasites (Figure 7A). After 12 hours of co-incubation, hepatocytes exposed to *T. brucei* showed a marked reduction in the expression of key gluconeogenic enzymes, *G6pc* and *Pck1*, relative to unexposed controls (Figure 7B). Consistently, hepatocytes co-cultured with parasites exhibited a significant decrease in glucose output (Figure 7C), confirming functional inhibition of gluconeogenesis.

Together, these data demonstrate that *T. brucei* directly acts on hepatocytes to repress the expression of gluconeogenic genes and glucose production.

Figure 7: *T. brucei* directly suppresses glucose production in hepatocytes

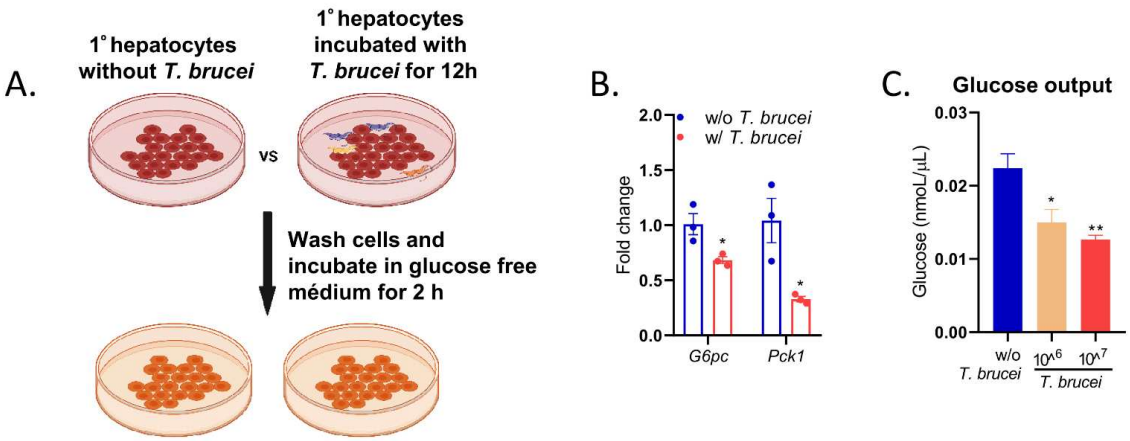

Figure 7**: *T. brucei* directly suppresses glucose production in hepatocytes**. **A.** Schematic showing the hepatocyte-*T. brucei* co-culture for assessment of glucose production in the hepatocytes. **B.** RT-qPCR quantification of gluconeogenic genes, *G6pc* and *Pck1,* in primary hepatocytes cultured with or without *T. brucei*. n = 3 each for hepatocytes cultured with or without *T. brucei*. **C.** Glucose output from primary hepatocytes pre-cultured with or without *T. brucei*. n = 4 each for hepatocytes cultured with or without *T. brucei*. Error bars represent the S.E.M. **P* < 0.05, ***P* < 0.01, *****P* < 0.0001. Statistical source data contain additional parameters.

Stimulating endogenous glucose production prolongs host survival

Because *T. brucei* infection profoundly suppresses hepatic gluconeogenesis, we hypothesised that restoring endogenous glucose production could ameliorate infection-induced hypoglycaemia and improve host survival. To test this, we supplemented the drinking water of infected mice with 5% glycerol, a direct gluconeogenic substrate. In naïve wild-type mice, glycerol supplementation did not alter feeding behaviour or fed-state glycaemia (Figure 8 A&B). Similarly, infected mice receiving glycerol-supplemented water consumed comparable amounts of food as untreated controls (Figure 8C).

Remarkably, glycerol supplementation in infected mice led to a sustained elevation in fed-state blood glucose during chronic stages of infection (Figure 8D). After overnight fasting, glycerol-treated mice also maintained significantly higher glycaemia on days 14 ($p < 0.01$), 21 ($p < 0.01$), and 28 ($p < 0.05$) post-infection (Figure 8E), confirming that the increased blood glucose resulted from enhanced endogenous glucose production stimulated by glycerol. Despite this metabolic improvement, glycerol supplementation did not alter parasitemia (Figure 8F), indicating that the effect was independent of parasite burden. Notably, glycerol-treated mice survived significantly longer, with mean survival extending from ~35 to 45 days ($p < 0.01$; Figure 8G).

In contrast, direct glucose supplementation (3% in drinking water) failed to increase blood glucose levels or improve survival (Supplementary Figure 3A–D), suggesting that exogenous glucose is either rapidly consumed or metabolically inaccessible during infection.

Together, these results demonstrate that stimulating gluconeogenesis through glycerol supplementation is sufficient to sustain systemic glycaemia and enhance host survival without affecting parasite load. This identifies impaired endogenous glucose production as a key driver of host vulnerability during *T. brucei* infection and highlights hepatic metabolic resilience as a critical determinant of disease tolerance.

Figure 8: Stimulating gluconeogenesis prolongs host survival

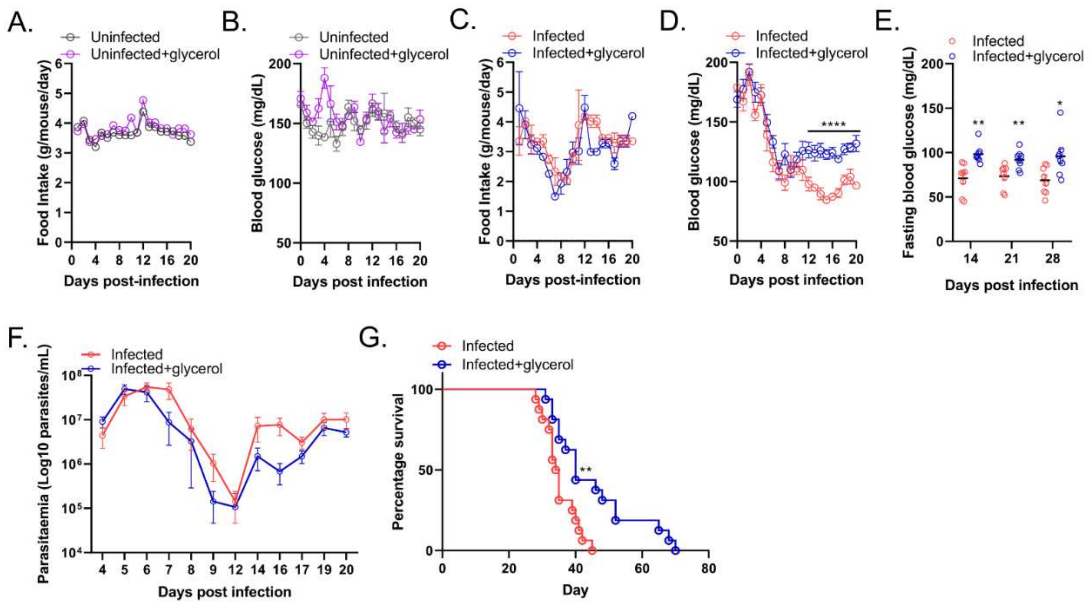

Figure 8**: Stimulating gluconeogenesis prolongs host survival**. **A.** Food intake of naïve WT mice supplemented with or without glycerol. **B.** Dynamics of blood glucose levels in the fed state of naïve WT mice supplemented with or without glycerol. n = 4 each for uninfected mice supplemented with or without glycerol. **C.** Food intake of infected WT mice supplemented with or without glycerol. **D.** Dynamics of blood glucose levels in the fed state of infected WT mice supplemented with or without glycerol. n = 14 each for infected mice supplemented with or without glycerol across 3 independent experiments. **E.** Overnight fasting blood glucose levels of infected WT mice supplemented with or without glycerol on day 14, 21, and 28 post-infection. n = 8 each for infected mice supplemented with or without glycerol across 2 independent experiments. **F.** Parasitaemia of infected WT mice supplemented with or without glycerol on selected days post-infection. n = 14 each for infected mice supplemented with or without glycerol across 3 independent experiments. **G.** Survival curves of infected WT mice supplemented with or without glycerol. n = 16 each for infected mice supplemented with or without glycerol across 3 independent experiments. Error bars represent the S.E.M. $*P < 0.05$, $**P < 0.01$, $****P < 0.0001$. Statistical source data contain additional parameters.

DISCUSSION

This study reveals that *T. brucei* infection profoundly impairs hepatic gluconeogenesis through a direct, parasite-driven suppression of host glucose production. Hypoglycaemia, a symptom reported in studies on *Trypanosoma*-infected hosts (5,29–31) has long been attributed to parasite glucose consumption. However, our data demonstrate that systemic hypoglycaemia instead emerges from an active inhibition of hepatic glucose synthesis, mostly mediated by the presence of the parasite.

Rethinking the Metabolic Pathology of African Trypanosomiasis

Because bloodstream-form *Trypanosoma brucei* relies heavily on glycolysis, it consumes glucose rapidly, and it can metabolise alternative carbon sources such as glycerol under restrictive conditions (13–15). It has seemed intuitive to attribute host hypoglycaemia directly to parasite competition for nutrient uptake. However, several conceptual and comparative considerations make glucose competition an inadequate explanation for hypoglycaemia. First, the scale of parasite biomass relative to total host glucose turnover is insufficient to drive systemic depletion (37), immune cells, skeletal muscle, and hepatocytes dominate endogenous glucose utilisation far beyond the metabolic demand of parasitaemia. Second, pathogens in other infections, such as *M. tuberculosis*, use glucose but overwhelmingly prioritise lipids and cholesterol *in vivo*, yet still induce hypoglycaemia through mechanisms that centre on hepatic metabolic reprogramming rather than substrate consumption (28). Third, viruses lack autonomous metabolism altogether, but some viruses can still impose profound suppression of gluconeogenesis (38). Collectively, these examples highlight a conceptual precedent: systemic hypoglycaemia is largely a host metabolic phenotype, not a reflection of pathogen carbon usage. Our finding that the hyper-parasitemia observed in RAG2$^{-/-}$ mice does not exacerbate hypoglycemia supports the conclusion that hypoglycemia is not correlated to parasite levels. Therefore African trypanosomiasis follows the paradigm of other infections, in which hypolglycemia is a host metabolic phenotype.

Parasites Supress Gluconeogenesis Causing Hypoglycaemia

In this work, we revealed that the central carbohydrate metabolic defect in African trypanosomiasis is a supression of hepatic gluconeogenesis. This conclusion emerged after ruling out dietary, intestinal, hormonal, and substrate availability explanations that commonly contribute to hypoglycaemia. We found a marked repression of gluconeogenic gene expression alongside functional failure of the liver to adequately convert classic precursors into glucose. Supression of gluconeogenesis is neither unique to trypanosomiasis nor unexpected in inflammatory disease. In diseases such as tuberculosis, sepsis, and malaria, gluconeogenesis is also constrained (26–28,36). Such suppression has implications for tolerance and nutritional immunity.

In a *T. brucei* infection, suppression of gluconeogenesis is mainly driven by a parasite-dependent mechanism. Hepatocyte-parasite co-culture demonstrates that *T. brucei* itself is sufficient to repress gluconeogenic gene expression and glucose output. Conversely, clearance of parasites *in vivo* restores gluconeogenesis despite persistent immune activation, indicating that parasite presence and not inflammation determines the metabolic state.

The discovery that *T. brucei* is a direct architect of host metabolic landscapes is conceptually novel. Although infections reshape host metabolic pathways, including affecting hepatic glucose output (26,27,36,44), this effect is usually driven by the host. In tuberculosis, sepsis, and malaria, repression of gluconeogenesis is driven by proinflammatory immune responses or the release of labile heme from the lysis of red blood cells. In these diseases the host reduces

endogenous glucose availability to limit pathogen access to key metabolites or modulate immune activity (39).

Suppression of host glucose production likely confers a selective advantage to *T. brucei*. It may reduce energetically costly immune responses, shift energy balance toward parasite-compatible states, or preserve alternative substrates such as glycerol that the parasite can exploit. It may also rewire host hormonal or metabolic circuits in ways that reduce resistance and enhance parasite persistence.

Enhancing Gluconeogenesis as a Tolerance Mechanism

The capacity to restore endogenous glucose production without altering parasite burden illuminates gluconeogenesis as a central determinant of disease tolerance (45). Supporting gluconeogenic flux through glycerol supplementation rather than supplying exogenous glucose sustains glycaemia because it bypasses insulin-mediated clearance and directly fuels hepatic glucose synthesis. This occurs because glycerol is a poor insulin secretagogue. Pancreatic β-cells lack sufficient glycerol kinase to metabolise glycerol for ATP generation, and glycerol infusion does not measurably elevate plasma insulin *in vivo* (46–48). In contrast, glucose supplementation provokes a rapid insulin surge, suppresses hepatic glucose production, and accelerates peripheral glucose disposal (49). Thus, glycerol uniquely elevates glycaemia without triggering counter-regulatory hormonal responses that would otherwise negate its benefit. This distinction underscores the physiological relevance of gluconeogenesis as the primary buffer against infection-induced hypoglycaemia and that supporting hepatic glucose production improves host survival even in the face of ongoing parasite replication.

Conclusion

Together, these findings provide a new conceptual model for the metabolic pathology of African trypanosomiasis. Hypoglycaemia stems from a parasite-driven, hepatocyte-intrinsic repression of gluconeogenesis. It does not stem from not from glucose consumption by the parasite nor from factors released during the adaptive immune response. This metabolic blockade compromises systemic energy homeostasis, shapes disease progression, and determines host survival. By showing that the liver's capacity to produce glucose governs tolerance to infection, this work highlights hepatic metabolic resilience as a fundamental axis of host defence and identifies gluconeogenesis as a promising target for adjunctive therapeutic strategies in systemic parasitic disease.

MATERIALS AND METHODS

Experimental Animals

8-10 week old male wild-type C57BL/6J mice were procured from Charles River Laboratories (France) and housed in a specific pathogen-free (SPF) barrier facility at the Gulbenkian Institute for Molecular Medicine (GIMM), Lisbon, Portugal. The genetically modified mice used are the $Rag2^{-/-}$ (IMSR_JAX:008449). The Mice were maintained under controlled environmental conditions with a 12-hour light/dark cycle, temperature set at 21–22°C, and humidity maintained at 45–65%, with unrestricted access to food and water unless otherwise specified. All experimental procedures were approved by the Orgão Responsável pelo Bem-estar Animal (ORBEA) of GIMM and the Direcção Geral de Alimentação e Veterinária (DGAV) (licenses 018889/2016 and 017549/2021), in accordance with European Directive 2010/63/EU on the protection of animals used for scientific purposes.

Parasite Infection and Monitoring

Mice were infected intraperitoneally (i.p.) with 2000 *T. brucei brucei* AnTat1.1^{E} 90-13 parasites suspended in 100 µL of HMI11 medium (ref). Uninfected mice were injected with 100 µL of HMI11 I.P. Parasitemia was monitored by collecting tail blood samples and quantifying parasite numbers using the Neubauer hemocytometer under a phase-contrast microscope. For terminal experiments, mice were euthanised at specific timepoints post-infection by CO_2 narcosis, blood was collected via cardiac puncture, and organs were perfused transcardially with 10mL of phosphate buffer saline (PBS).

Glucose and Metabolic Tolerance Tests

Sucrose Tolerance Test (STT): to assess sucrose digestion and glucose absorption and clearance, mice were fasted for 6h during the light phase and were gavaged with 2 g/kg body weight of sucrose (Sigma-Aldrich, S9378-1KG), and blood glucose levels were measured via tail puncture at 0, 15, 30, 60, and 120 min using an Accu-Chek glucometer (Roche, Germany).

Intraperitoneal Glucose Tolerance Test (IPGTT): to assess glucose tolerance and clearance, mice were fasted for 6h during the light phase and were administered 1 g/Kg glucose (Sigma, G8270-1KG) intraperitoneally (i.p.), with glycaemia monitored at the same time points as in STT.

Pyruvate Tolerance Test (PTT): To assess pyruvate–mediated gluconeogenesis, mice were fasted overnight and were administered 2 g/Kg body weight sodium pyruvate (Sigma, P2256-100G) i.p., and glycaemia levels were recorded at the same time as in STT.

Glycerol Tolerance Test (GTT): To assess glycerol–mediated gluconeogenesis, mice were i.p. injected with 1 g/Kg glycerol (Abcam, ab285399), and glycaemia was monitored over time as in STT.

Biochemical Analysis

Blood glucose and lactate were measured from blood collected by vial tail puncture from infected and uninfected mice fasted for 4 h using the Accu-Chek glucometer and Accutrend Plus (Roche, Germany), respectively. Blood collected

via cardiac puncture after CO_2 narcosis was centrifuged to collect serum. Pyruvate (Abcam, ab65342) and glycerol (Sigma, MAK117) levels were quantified using colourimetric assays. Insulin (ALPCO, 80-INSMSU-E10) and glucagon (R&D Systems, DGCG0) levels were measured by ELISA.

mRNA Sequencing

Following mouse euthanasia and perfusion, as described above, livers were collected from uninfected and infected mice at days 6, 10, and 22 post-infection, flash-frozen in liquid nitrogen, and stored at -80°C. Approximately 100mg of tissue was submerged in 1mL TRIzol with zirconia beads and mechanically homogenised in a bead beater. Subsequently, total RNA was extracted according to TRIzol manufacturer's protocol (supplier?). RNA concentration was quantified by Qubit HS RNA (Invitrogen UK), and integrity was assessed first by gel electrophoresis on a 1.5% agarose gel, run for 45 minutes at 100V, and subsequently in the Agilent 4200 TapeStation (Agilent, UK), at the DeepSeq Facility of the University of Nottingham. RNA with RIN values above 7.0 was used to prepare cDNA libraries using the Lexogen QuantSeq 3´ FWD library kit (Lexogen, UK) and sequenced as single-end 75bp reads multiplexed on a single lane of the Illumina NextSeq 500 platform, using the NextSeq 500 High Output v2.5 75 Cycle Kit (Illumina, UK).

Transcriptomic analysis

Sequencing quality was assessed with FastQC v. 0.11.5 (50) before and after trimming with BBDuck v. 35.92 (51). Reads shorter than 20 base pairs and those aligning to the *T. brucei* TREU 927 genome (52) were discarded. Remaining reads were aligned to the mouse reference genome (GRCm38/mm10) using STAR (53). Mapping output files were processed with SAMtools v. 0.6.0 (54), and read counts were estimated with HTSeq-count v. 0.11.2 (55). Only uniquely mapping reads were considered. Differential expression analysis was performed in R, using edgeR (56) and limma-voom (57). Genes with less than 10 reads were ignored, and differentially expressed genes were defined as those with an absolute $\log_2$ fold change ≥ 1 and an adjusted p-value < 0.05. Gene Ontology (GO) enrichment analysis was performed with PANTHER version 19.0 (58) for GO-Slim Biological Process with Fisher's exact test and Bonferroni correction. Gene set enrichment analysis was conducted with GSEA version 4.3.3 (59).

Real-Time Quantitative PCR (RT-qPCR)

To confirm some of the differentially expressed genes from the total liver RNA-seq, livers from uninfected and infected mice on days 3, 5, 7, 14, 21, and 28 post infection was collected from perfused mice and snap-frozen in liquid nitrogen. RNA were extracted from the tissues using the NZYTech total RNA isolation kit (NZYTech, MB13402). cDNA was synthesized from total RNA using the Xpert cDNA synthesis kit (GRiSP, GK80.0100). RT-qPCR was performed on a QuantStudio Real-Time PCR System (Applied Biosystems, USA) with SYBR Green Master Mix (GRiSP, GE20.5100). Relative expression levels were normalized to GAPDH and analyzed using the $^{\Delta\Delta}$Ct method. Primer sequences are listed in Supplementary File 2.

Flow cytometry

Longitudinal characterization of circulating immune cells was performed using 10 µL of peripheral blood collected from the mouse tail vein into PBS containing 10 U/mL heparin. Following two consecutive 5-minute incubations in ammonium–chloride–potassium (ACK) lysis buffer to remove erythrocytes, cells were washed with PBS supplemented with 2% fetal bovine serum (PBS/2% FBS). Samples were then incubated with Fc block (eBioscience, Thermo Fisher Scientific) for 10 minutes at 4–8 °C to prevent nonspecific Fc receptor binding. Surface staining was performed for 20 minutes at 4–8 °C using a fixable viability dye (eFluor 780, eBioscience, Thermo Fisher Scientific), to exclude dead cells, as well as the following fluorochrome-conjugated anti-mouse monoclonal antibodies (BioLegend or BD Biosciences): CD45 Alexa Fluor 700 (clone 30-F11), CD19 Brilliant Violet 570 (clone 6D5), TCRβ PE-Cy7 (clone H57-597), CD4 BD Horizon BUV805 (clone RM4-5), CD8α BD Horizon BUV496 (clone 53-6.7), CD62L Brilliant Violet 510 (clone MEL-14), and CD44 Brilliant Violet 785 (clone IM7). Stained cells were resuspended in PBS/2% FBS, acquired on a Cytek Aurora spectral cytometer (Cytek Biosciences), and analyzed using FlowJo v10 (BD). Gating strategy for CD4+ T cells, CD8+ T cells, and effector/effector memory (T_{EM}) CD4+ and CD8+ T cell subsets are shown in Supplementary Figure 3A.

Parasite clearance

On day 14 post infection, infected and uninfected mice were treated intravenously with 5 mg/Kg body weight of melarsoprol (Aventis, France). Melarsoprol was diluted in sterile propylene glycol (26% of final solution) (Sigma, W294004-1KG-K) and PBS (70% of final solution).

Primary hepatocyte Isolation

Primary Primary hepatocytes were isolated from adult C57BL/6 mice using a Liberase Blendzyme 3 recombinant collagenase (Roche Diagnostics) perfusion method (60). Mice were anaesthetized with ketamine (100 mg/kg) and xylazine (10 mg/kg) and positioned supine for surgery. After laparotomy, the inferior vena cava was exposed and cannulated for in situ liver perfusion using a peristaltic pump. The liver was first perfused with a perfusion buffer composed of Hank's balanced salt solution (HBSS; without Ca^{2+}, Mg^{2+}, and phenol red) (Gibco, 14175-095) supplemented with 0.5 mM EDTA and 25 mM hepes to remove blood and chelate divalent cations. This was followed by perfusion with a digestion buffer containing HBSS (with Ca^{2+}, Mg^{2+}, and phenol red) (Gibco, 24020-117) supplemented with hepes (25 mM), and 40 µg/mL liberase (Roche) to enzymatically dissociate hepatocytes. After complete perfusion, the liver was excised, transferred to a dish containing digestion buffer, gently disaggregated, and filtered through a 100 µm cell strainer into a 50 mL tube. The suspension was centrifuged at 30 × g for 3 min at room temperature (RT), and the supernatant discarded. The pellet was resuspended in 25 mL digestion buffer without liberase and centrifuged through 25 mL Percoll (Sigma, P4937) at 70 × g for 10 min at RT to enrich for viable hepatocytes. The resulting pellet was resuspended in Primary Hepatocyte Culture Medium (PHCM) consisting of William's E medium (with phenol red) (Gibco, 11514466) supplemented with 1% L-glutamine, 1% penicillin–streptomycin, and 4% fetal bovine serum (FBS). The hepatocyte suspension was filtered again through a 100

μm strainer, centrifuged (30 × g, 3 min, RT), and the final pellet resuspended in PHCM. Cells were counted and plated on collagen-coated 12-well plates at a density of 3×10^5 cells per well, then incubated at 37 °C with 5% CO_2. After 3 h of attachment, the medium was replaced with PHCM supplemented with 0.1% gentamicin and 0.3% fungizone. Cells were maintained for approximately 18-24 h to allow complete adhesion prior to experimental treatments.

Hepatocyte-parasite co-culture

After complete adhesion (~12 h) of primary hepatocytes, the culture medium was replaced with a mixed medium composed of 50% Primary Hepatocyte Culture Medium (PHCM) and 50% parasite culture medium (HMI-11). Hepatocytes were then incubated in this medium with or without bloodstream-form *T. brucei* at a density of 1×10^6 or 1×10^7 parasites/mL for 12 h at 37 °C and 5% CO_2. Following co-culture, the medium was aspirated, and the wells were gently washed twice with Dulbecco's Modified Eagle Medium (DMEM) without glucose to remove residual parasites and substrate. Hepatocytes were then incubated in fresh DMEM (without glucose) for 2 h to assess endogenous glucose production. At the end of the incubation, the culture supernatant was collected, clarified by centrifugation (300 × g, 5 min), and the glucose concentration was quantified colourimetrically using the Glucose Assay Kit (Abcam, ab65333) according to the manufacturer's instructions.

Glucose and glycerol supplementation

The drinking water of mice was supplemented with either 3% (w/v) D-glucose (Sigma, G8270-1KG) or 5% (v/v) glycerol (Abcam, ab285399). Supplementation began on the day of infection and continued throughout the experimental period. The solutions were freshly prepared and replaced every 48 h to prevent microbial growth and ensure consistent substrate availability.

Statistical Analysis

Transcriptomic data were analysed in R as described in the corresponding section. The remaining data were analysed using GraphPad Prism 9. Normality was assessed with the Shapiro-Wilk test. For comparisons between two groups, unpaired two-tailed Student's t-tests were used. For multiple comparisons, one-way or two-way ANOVA with Bonferroni post-hoc correction was applied. Survival analysis was performed using the Kaplan-Meier method with log-rank tests. Data are presented as mean ± SEM, with significance defined as $p < 0.05$.

ACKNOWLEDGEMENTS

We are thankful to the Figueiredo lab members for helpful discussions. We are also grateful to Andreia Mósca (Prudencio Lab, GIMM) and Sofia Marques (Mota Lab, GIMM). We acknowledge the staff of GMM's rodent and flow cytometry facilities for their excellent animal husbandry & welfare services, and their technical expertise and operational support, respectively. Illustrations were made using BioRender. This work was supported by the Fundação Ciência e a Tecnologia (FCT), Portugal (2023.11294.PEX to AA). The Marie Skłodowska-Curie Individual Standard European Fellowship, under grant agreement no. 839960 and "la Caixa"

Foundation, Spain (ID 10001043) through a Junior Leader Postdoctoral Fellowship (LCF/BQ/PR23/11980034) to SSP. The la Caixa Foundation Health Program, Spain (HR24-00288), and European Research Council (ERC) under the European Union's Horizon 2020 research and innovation programme (grant agreement no. 771714) to LMF.

DECLARATION OF GENERATIVE AI AND AI-ASSISTED TECHNOLOGIES IN THE WRITING PROCESS

During the preparation of this work, the author(s) used ChatGPT 5.1 in order to improve the readability of the manuscript. After using this tool, the author(s) reviewed and edited the content as needed and take(s) full responsibility for the content of the published article.

REFERENCES

1. Energetic Trade-Offs and Hypometabolic States Promote Disease Tolerance - ScienceDirect [Internet]. [cited 2025 Jan 3]. Available from: https://www.sciencedirect.com/science/article/pii/S0092867419301138#bib35
2. Borer ET, Kendig AE, Holt RD. Feeding the fever: Complex host-pathogen dynamics along continuous resource gradients. Ecol Evol. 2023 July 25;13(7):e10315.
3. Troha K, Ayres JS. Metabolic adaptations to infections at the organismal level. Trends Immunol. 2020 Feb;41(2):113–25.
4. Lochmiller RL, Deerenberg C. Trade-offs in evolutionary immunology: just what is the cost of immunity? Oikos. 2000;88(1):87–98.
5. Ojo RJ, Paul GM, Magellan DD, Dangara DN, Gyebi G. Trypanosoma brucei brucei Induced Hypoglycaemia Depletes Hepatic Glycogen and Altered Hepatic Hexokinase and Glucokinase Activities in Infected Mice. Acta Parasit. 2022 Sept 1;67(3):1097–106.
6. Zijlmans W, Jitan J, Ackermans MT, Serlie MJ, van Kempen AAMW, Sauerwein HP. Type of infectious disease affects glucose metabolism and liver glycogen content in Surinamese children: malaria vs. pneumonia. J Pediatr Endocrinol Metab. 2013;26(3–4):293–9.
7. Machado H, Hofer P, Zechner R, Smith TK, Figueiredo LM. Adipocyte lipolysis protects mice against Trypanosoma brucei infection. Nat Microbiol. 2023 Nov;8(11):2020–32.
8. Sinton MC, Kajimura S. From fat storage to immune hubs: the emerging role of adipocytes in coordinating the immune response to infection. The FEBS Journal [Internet]. [cited 2025 Jan 3];n/a(n/a). Available from: https://onlinelibrary.wiley.com/doi/abs/10.1111/febs.17302
9. Xu X, Qi X, Shao Y, Li Y, Fu X, Feng S, et al. High glucose induced-macrophage activation through TGF-β-activated kinase 1 signaling pathway. Inflamm Res. 2016 Aug 1;65(8):655–64.

10. Chen C, Cao J, Gao Y, Xie X, Zhao Z, Yuan Q, et al. High glucose promotes macrophage M1 polarization through miR-32/Mef2d/cAMP signaling pathway. Genes & Diseases. 2024 Mar 1;11(2):539–41.
11. Hidalgo MA, Carretta MD, Burgos RA. Long Chain Fatty Acids as Modulators of Immune Cells Function: Contribution of FFA1 and FFA4 Receptors. Front Physiol [Internet]. 2021 July 1 [cited 2025 July 9];12. Available from: https://www.frontiersin.org/journals/physiology/articles/10.3389/fphys.2021.668330/full
12. Radzikowska U, Rinaldi AO, Çelebi Sözener Z, Karaguzel D, Wojcik M, Cypryk K, et al. The Influence of Dietary Fatty Acids on Immune Responses. Nutrients. 2019 Dec 6;11(12):2990.
13. Creek DJ, Mazet M, Achcar F, Anderson J, Kim DH, Kamour R, et al. Probing the Metabolic Network in Bloodstream-Form Trypanosoma brucei Using Untargeted Metabolomics with Stable Isotope Labelled Glucose. PLOS Pathogens. 2015 Mar 16;11(3):e1004689.
14. Haanstra JR, van Tuijl A, van Dam J, van Winden W, Tielens AGM, van Hellemond JJ, et al. Proliferating bloodstream-form *Trypanosoma brucei* use a negligible part of consumed glucose for anabolic processes. International Journal for Parasitology. 2012 June 1;42(7):667–73.
15. Pineda E, Thonnus M, Mazet M, Mourier A, Cahoreau E, Kulyk H, et al. Glycerol supports growth of the Trypanosoma brucei bloodstream forms in the absence of glucose: Analysis of metabolic adaptations on glycerol-rich conditions. PLoS Pathog. 2018 Nov 1;14(11):e1007412.
16. Bringaud F, Plazolles N, Pineda E, Asencio C, Villafraz O, Millerioux Y, et al. Glycerol, a possible new player in the biology of trypanosomes. PLoS Pathog. 2021 Dec 2;17(12):e1010035.
17. Counihan NA, Modak JK, de Koning-Ward TF. How Malaria Parasites Acquire Nutrients From Their Host. Front Cell Dev Biol. 2021 Mar 25;9:649184.
18. Sood C, Verma JK, Basak R, Kapoor A, Gupta S, Mukhopadhyay A. Leishmania highjack host lipid body for its proliferation in macrophages by overexpressing host Rab18 and TRAPPC9 by downregulating miR-1914-3p expression. PLoS Pathog. 2024 Feb 27;20(2):e1012024.
19. Carbohydrate Digestion and Absorption. Nutrition Reviews. 1963 Sept 1;21(9):279–81.
20. Shah A, Wondisford FE. Gluconeogenesis Flux in Metabolic Disease. Annual Review of Nutrition. 2023 Aug 21;43(Volume 43, 2023):153–77.
21. Röder PV, Wu B, Liu Y, Han W. Pancreatic regulation of glucose homeostasis. Exp Mol Med. 2016 Mar;48(3):e219–e219.
22. Han HS, Kang G, Kim JS, Choi BH, Koo SH. Regulation of glucose metabolism from a liver-centric perspective. Exp Mol Med. 2016 Mar;48(3):e218–e218.
23. Ekberg K, Landau BR, Wajngot A, Chandramouli V, Efendic S, Brunengraber H, et al. Contributions by kidney and liver to glucose production in the postabsorptive state and after 60 h of fasting. Diabetes. 1999 Feb 1;48(2):292–8.
24. Hatting M, Tavares CDJ, Sharabi K, Rines AK, Puigserver P. Insulin regulation of gluconeogenesis. Annals of the New York Academy of Sciences. 2018;1411(1):21–35.

25. Colberg SR. Why Glucagon Matters for Hypoglycemia and Physical Activity in Individuals With Type 1 Diabetes. Front Clin Diabetes Healthc. 2022 July 8;3:889248.
26. Weis S, Carlos AR, Moita MR, Singh S, Blankenhaus B, Cardoso S, et al. Metabolic Adaptation Establishes Disease Tolerance to Sepsis. Cell. 2017 June 15;169(7):1263-1275.e14.
27. Ramos S, Ademolue TW, Jentho E, Wu Q, Guerra J, Martins R, et al. A hypometabolic defense strategy against malaria. Cell Metabolism. 2022 Aug 2;34(8):1183-1200.e12.
28. Das MK, Savidge B, Pearl JE, Yates T, Miles G, Pareek M, et al. Altered hepatic metabolic landscape and insulin sensitivity in response to pulmonary tuberculosis. PLOS Pathogens. 2024 Sept 27;20(9):e1012565.
29. Wang Y, Utzinger J, Saric J, Li JV, Burckhardt J, Dirnhofer S, et al. Global metabolic responses of mice to Trypanosoma brucei brucei infection. Proceedings of the National Academy of Sciences. 2008 Apr 22;105(16):6127–32.
30. Deschamps JY, Desquesnes M, Dorso L, Ravel S, Bossard G, Charbonneau M, et al. Refractory hypoglycaemia in a dog infected with Trypanosoma congolense. Parasite. 2016;23:1.
31. Nieman RE, Kelly JJ, Waskin HA. Severe African trypanosomiasis with spurious hypoglycemia. J Infect Dis. 1989 Feb;159(2):360–2.
32. Ojo RJ, Paul GM, Magellan DD, Dangara DN, Gyebi G. Trypanosoma brucei brucei Induced Hypoglycaemia Depletes Hepatic Glycogen and Altered Hepatic Hexokinase and Glucokinase Activities in Infected Mice. Acta Parasit. 2022 Sept 1;67(3):1097–106.
33. Röder PV, Wu B, Liu Y, Han W. Pancreatic regulation of glucose homeostasis. Exp Mol Med. 2016 Mar;48(3):e219–e219.
34. Zhang X, Yang S, Chen J, Su Z. Unraveling the Regulation of Hepatic Gluconeogenesis. Front Endocrinol [Internet]. 2019 Jan 24 [cited 2025 June 16];9. Available from: https://www.frontiersin.org/journals/endocrinology/articles/10.3389/fendo.2018.00802/full
35. Wang MY, Zhang Z, Zhao S, Onodera T, Sun XN, Zhu Q, et al. Downregulation of the kidney glucagon receptor, essential for renal function and systemic homeostasis, contributes to chronic kidney disease. Cell Metabolism. 2024 Mar 5;36(3):575-597.e7.
36. de Souza Galia WB, Biazi GR, Frasson-Uemura IG, Miksza DR, Zaia CTBV, Zaia DAM, et al. Gluconeogenesis is reduced from alanine, lactate and pyruvate, but maintained from glycerol, in liver perfusion of rats with early and late sepsis. Cell Biochemistry and Function. 2021;39(6):754–62.
37. Poulin R, George-Nascimento M. The scaling of total parasite biomass with host body mass. International Journal for Parasitology. 2007 Mar 1;37(3):359–64.
38. Davis LE, Woodfin BM, Tran TQ, Caskey LS, Wallace JM, Scremin OU, et al. The influenza B virus mouse model of Reye's syndrome: pathogenesis of the hypoglycaemia. Int J Exp Pathol. 1993 June;74(3):251–8.
39. Murdoch CC, Skaar EP. Nutritional immunity: the battle for nutrient metals at the host–pathogen interface. Nat Rev Microbiol. 2022 Nov;20(11):657–70.

40. Goto M, Yoshioka T, Battelino T, Ravindranath T, Zeller WP. TNFα Decreases Gluconeogenesis in Hepatocytes Isolated from 10-Day-Old Rats. Pediatr Res. 2001 Apr;49(4):552–7.
41. Yerkovich ST, Rigby PJ, Fournier PA, Olynyk JK, Yeoh GCT. Kupffer cell cytokines interleukin-1β and interleukin-10 combine to inhibit phosphoenolpyruvate carboxykinase and gluconeogenesis in cultured hepatocytes. The International Journal of Biochemistry & Cell Biology. 2004 Aug 1;36(8):1462–72.
42. Metzger S, Nusair S, Planer D, Barash V, Pappo O, Shilyansky J, et al. Inhibition of Hepatic Gluconeogenesis and Enhanced Glucose Uptake Contribute to the Development of Hypoglycemia in Mice Bearing Interleukin-1β- Secreting Tumor. Endocrinology. 2004 Nov 1;145(11):5150–6.
43. Tanaka H, Nishikawa Y, Fukushima T, Taniguchi A, Fujita Y, Tsuda K, et al. Lipopolysaccharide inhibits hepatic gluconeogenesis in rats: The role of immune cells. Journal of Diabetes Investigation. 2018;9(3):494–504.
44. Van Wyngene L, Vandewalle J, Libert C. Reprogramming of basic metabolic pathways in microbial sepsis: therapeutic targets at last? EMBO Molecular Medicine. 2018 Aug;10(8):e8712.
45. Medzhitov R, Schneider DS, Soares MP. Disease tolerance as a defense strategy. Science. 2012 Feb 24;335(6071):936–41.
46. Noel RJ, Antinozzi PA, McGarry JD, Newgard CB. Engineering of glycerol-stimulated insulin secretion in islet beta cells. Differential metabolic fates of glucose and glycerol provide insight into mechanisms of stimulus-secretion coupling. J Biol Chem. 1997 July 25;272(30):18621–7.
47. Carroll KF, Nestel PJ. Effect of Long-chain Triglyceride on Human Insulin Secretion. Diabetes. 1972 Sept 1;21(9):923–9.
48. Antinozzi PA, Ishihara H, Newgard CB, Wollheim CB. Mitochondrial Metabolism Sets the Maximal Limit of Fuel-stimulated Insulin Secretion in a Model Pancreatic Beta Cell: A SURVEY OF FOUR FUEL SECRETAGOGUES *. Journal of Biological Chemistry. 2002 Apr 5;277(14):11746–55.
49. Edgerton DS, Kraft G, Smith M, Farmer B, Williams PE, Coate KC, et al. Insulin's direct hepatic effect explains the inhibition of glucose production caused by insulin secretion. JCI Insight. 2(6):e91863.
50. Babraham Bioinformatics - FastQC A Quality Control tool for High Throughput Sequence Data [Internet]. [cited 2025 Nov 1]. Available from: https://www.bioinformatics.babraham.ac.uk/projects/fastqc/
51. Bushnell B. BBMap: A Fast, Accurate, Splice-Aware Aligner. 2014 Mar 19 [cited 2025 Nov 1]; Available from: https://escholarship.org/uc/item/1h3515gn
52. Berriman M, Ghedin E, Hertz-Fowler C, Blandin G, Renauld H, Bartholomeu DC, et al. The Genome of the African Trypanosome Trypanosoma brucei. Science. 2005 July 15;309(5733):416–22.
53. Dobin A, Davis CA, Schlesinger F, Drenkow J, Zaleski C, Jha S, et al. STAR: ultrafast universal RNA-seq aligner. Bioinformatics. 2013 Jan 1;29(1):15–21.
54. Li H, Handsaker B, Wysoker A, Fennell T, Ruan J, Homer N, et al. The Sequence Alignment/Map format and SAMtools. Bioinformatics. 2009 Aug 15;25(16):2078–9.
55. Anders S, Pyl PT, Huber W. HTSeq—a Python framework to work with high-throughput sequencing data. Bioinformatics. 2015 Jan 15;31(2):166–9.

56. Robinson MD, McCarthy DJ, Smyth GK. edgeR: a Bioconductor package for differential expression analysis of digital gene expression data. Bioinformatics. 2010 Jan 1;26(1):139–40.
57. Ritchie ME, Phipson B, Wu D, Hu Y, Law CW, Shi W, et al. limma powers differential expression analyses for RNA-sequencing and microarray studies. Nucleic Acids Res. 2015 Apr 20;43(7):e47.
58. Thomas PD, Ebert D, Muruganujan A, Mushayahama T, Albou LP, Mi H. PANTHER: Making genome-scale phylogenetics accessible to all. Protein Science. 2022;31(1):8–22.
59. Subramanian A, Tamayo P, Mootha VK, Mukherjee S, Ebert BL, Gillette MA, et al. Gene set enrichment analysis: A knowledge-based approach for interpreting genome-wide expression profiles. Proceedings of the National Academy of Sciences. 2005 Oct 25;102(43):15545–50.
60. Halpern KB, Shenhav R, Matcovitch-Natan O, Tóth B, Lemze D, Golan M, et al. Single-cell spatial reconstruction reveals global division of labour in the mammalian liver. Nature. 2017 Feb;542(7641):352–6.

SUPPLEMENTAL FIGURES

Supplementary figure 1: Endogenous glucose production is impaired in mice infected with *T. brucei*

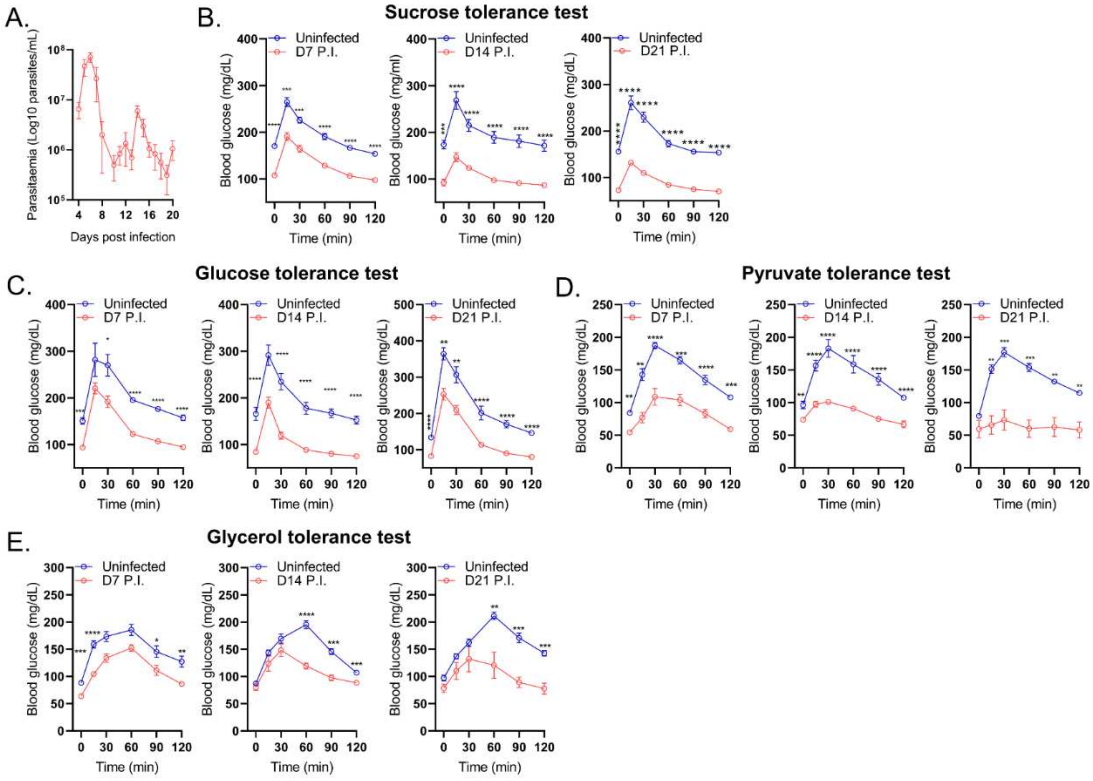

Supplementary Figure 1: **Endogenous glucose production is impaired in mice infected with *T. brucei*. A.** Dynamics of parasitaemia in WT mice infected with *T. brucei*. **B.** Change in blood glucose during the sucrose tolerance test in uninfected and infected WT mice. n = 6 uninfected and n = 6 infected mice on day 7, n = 7 uninfected and n = 9 infected mice on day 14, and n = 6 uninfected and n = 6 infected mice on day 21 post-infection, examined over 2 independent experiments. **C.** Change in blood glucose during glucose tolerance test in uninfected and infected WT mice. n = 6 uninfected and n = 6 infected mice on day 7, n = 6 uninfected and n = 8 infected mice on day 14, and n = 8 uninfected and n = 8 infected mice on day 21 post-infection, examined over 2 independent experiments. **D.** Change in blood glucose during the pyruvate tolerance test in uninfected and infected WT mice. n = 6 uninfected and n = 6 infected mice on day 7, n = 6 uninfected and n = 8 infected mice on day 14, and n = 6 uninfected and n = 6 infected mice on day 21 post-infection, examined over 2 independent experiments. **E.** Change in blood glucose during the glycerol tolerance test in uninfected and infected WT mice. n = 6 uninfected and n = 6 infected mice on day 14, and n = 6 uninfected and n = 5 infected mice on day 21 post-infection examined over 2 independent experiments. Error bars represent the S.E.M. *$P < 0.05$, **$P < 0.01$, ****$P < 0.0001$. Statistical source data contain additional parameters.

Supplementary Figure 2: Persistent imune activation despite parasite clearance

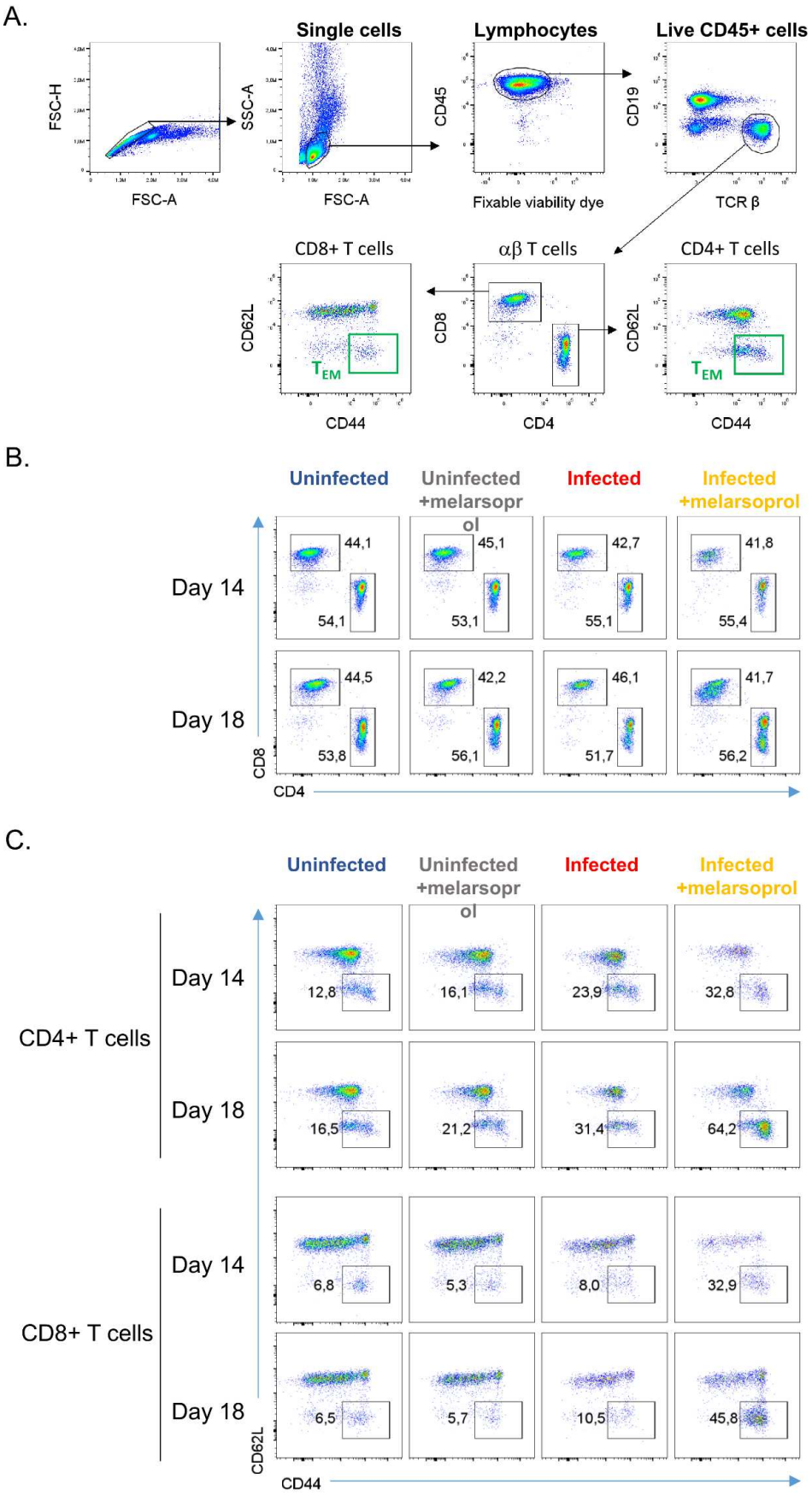

320

Supplementary Figure 2: **Persistent immune activation despite parasite clearance. A.** Flow cytometry gating strategy used to analyze CD4+ and CD8+ T cells, as well as effector/effector memory (T_{EM}) CD4+ and CD8+ T cell subsets, in peripheral blood from uninfected or *T. brucei*-infected mice, treated or not with melarsoprol on day 15, and analyzed on days 14 and 18 post-infection **B.** Representative dot plots of circulating CD4+ and CD8+ T cells in experimental groups, gated within αβ T cells, as defined in A. **C.** Representative dot plots of effector/effector memory (T_{EM}) CD4+ and CD8+ T cell subsets in experimental groups, gated within CD4+ or CD8+ αβ T cells, as defined in A.

Supplementary Figure 3: Glucose supplementation have no impact on host survival

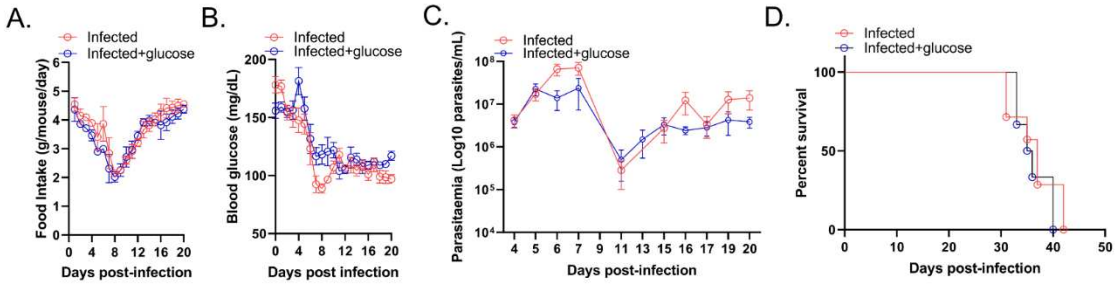

Supplementary Figure 3: **Glucose supplementation has no impact on host survival**. **A.** Food intake dynamics of infected WT mice supplemented with or without glucose. **B.** Blood glucose dynamics in infected WT mice supplemented with or without glucose. n = 7 for infected mice and n = 6 for infected mice supplemented with glucose. **C.** Parasitaemia in infected WT mice supplemented with or without glucose. n = 7 for infected mice and n = 6 for infected mice supplemented with glucose. **D.** Survival curves of infected WT mice supplemented with or without glucose. n = 7 for infected mice and n = 6 for infected mice supplemented with glucose. Error bars represent the S.E.M. *$P < 0.05$, **$P < 0.01$, ****$P < 0.0001$. Statistical source data contain additional parameters.

Supplementary Files

This is a list of supplementary files associated with this preprint. Click to download.

- SupplementaryFile2primersequence.xlsx
- Supplementaryfile1RNASeq.xlsx